Technical Note

1971-3

ELF Propagation Study

(Phase 1 — Summer 1970)

D. P. White
D. K. Willim

11 January 1971

Prepared for the Department of the Navy
under Electronic Systems Division Contract F19628-70-C-0230 by

Lincoln Laboratory

MASSACHUSETTS INSTITUTE OF TECHNOLOGY

Lexington, Massachusetts

MASSACHUSETTS INSTITUTE OF TECHNOLOGY

LINCOLN LABORATORY

ELF PROPAGATION STUDY
(PHASE 1 – SUMMER 1970)

D. P. WHITE

D. K. WILLIM

Group 66

TECHNICAL NOTE 1971-3

11 JANUARY 1971

LEXINGTON MASSACHUSETTS

The work reported in this document was performed at Lincoln Laboratory, a center for research operated by Massachusetts Institute of Technology. The work was sponsored by the Department of the Navy under Air Force Contract F19628-70-C-0230.

ABSTRACT

With the availability of an ELF transmitter (the Bravo test facility at Clam Lake, Wisconsin) it now becomes feasible to make far-field field strength measurements at the lower ELF frequencies. Field strength measurements were made in Hawaii and California at 45 and 75 Hz in an attempt to determine the east-west attenuation rate under daytime or nighttime conditions over the propagation path. As a result of high atmospheric noise conditions and a low transmitted power level, the relatively large uncertainty in signal estimates makes accurate estimation of α impossible. However, the data indicate a daytime east to west attenuation rate between 0.7 and 1.2 db/Mm and a nighttime rate between 1.0 and 1.8 db/Mm.

Future experiments are being planned to refine the estimates of α to within ± 0.2 db/Mm.

Accepted for the Air Force
Joseph R. Waterman, Lt. Col., USAF
Chief, Lincoln Laboratory Project Office

TABLE OF CONTENTS

The authors and M. I. T. Lincoln Laboratory would like to express their appreciation for the co-operation received by the staff of the two sites where measurements were conducted. The availability of two sites with low interference properties on the same great circle path was a cornerstone in the success of the experiment. In particular we would like to recognize the co-operation of Arthur Hewett of Hawaii Volcanoes National Park and Richard Montague of the Hat Creek Ranger District, California.

I. INTRODUCTION

Over a three week period covering July 6 through July 24 (1970), the test facility transmitter in Wisconsin was tasked to transmit a sinusoidal signal for four hour intervals during which the Wisconsin - Hawaii propagation path was either entirely in daylight or in nighttime conditions. Transmissions were scheduled from either 0100 to 0500 or 1300 to 1700 hours Central Daylight Savings Time. For the first two weeks transmissions were scheduled at 45 Hz and for the third week at 75 Hz. The antenna current level was 150A*. Receivers were positioned at Hawaii's Volcano National Park and at Hat Creek, California along a great circle path which includes the Wisconsin transmitter facility.

Until recently theoretical estimates and sferic measurements of the attenuation coefficient (α) at 45 Hz resulted in a range of values between 0.6 and 0.8 db/Mm which were assumed applicable under nighttime as well as daytime conditions and were virtually independent of propagation direction. Recent theoretical considerations, which incorporate the effects of ions, have suggested nighttime attenuation rates of the order of 1.1 to 1.2 db/Mm [1,2]. These recent theoretical results still indicate only a very small directional dependence (i.e., $\sim$ 0.1 db/Mm difference in nighttime attenuation coefficient for propagation from east to west versus that of west to east). However, two recent station sferic measurements by Smith [3] and Hughes [4] have been interpreted to indicate east to west attenuation coefficients for daytime conditions which are greater than 2.0 db/Mm. As a result of this present uncertainty in knowledge of the attenuation coefficient's diurnal as well as directional dependence, it becomes difficult to decide on an appropriate sizing for an ELF communications system. Clearly a series of measurements to determine the attenuation coefficient within a few tenths of a db/Mm in various propagation directions and for different ionospheric conditions would be invaluable in making an economical system sizing.

*Except for the nighttime transmissions on July 9-10 and July 10-11.

However, for the present radiated power levels this would be an extremely difficult measurement for reasons which will be explained more fully in the remainder of the report. With the experimental configuration as set up in Hawaii and California it is possible to determine whether an east to west daytime attenuation coefficient greater than 2.0 db/Mm did exist as claimed by Hughes. Accordingly the main purpose of the recently completed measurements was to show that extremely large values of attenuation coefficient (in excess of 2.0 db/Mm) were not in evidence. A subsidiary purpose was to test experimental techniques which are to be used in a future expanded series of measurements which will attempt to measure α within a few tenths of a db/Mm. These future experiments are described in detail in another report.

It should be recognized that α is just one of the parameters in the analytic expression for field strength at any point in the earth ionosphere cavity. The analytic expression most commonly used is an asymptotic form of the exact solution of propagation in a cavity bounded by two concentric spherical surfaces representing the earth and the "effective" lower boundary of the ionosphere. Each of these surfaces is assumed to have a uniform conductivity over its entire surface. Moreover the transmitter is assumed to be a short vertical dipole. In reality however the earth's conductivity varies from point to point on its surface, the antenna is in fact a horizontal line and the ionosphere changes significantly from nighttime to daylight conditions and has a continuous profile with height rather than a step discontinuity. Rather than attempt a full wave solution on a realistic model it has been relatively fruitful to make intuitive modifications to the ideal homogeneous concentric cavity solution. The main problem of course is to determine the magnitude of error that these approximations introduce. Wait[5] provides a good review of the various approximations for near field, far fields, field near antipode etc. In the far field and away from the antipode, the horizontal magnetic intensity for the direct component traveling along the shorter segment of the great circle joining the transmitter and receiver is given by

$$H_\varphi = \frac{(IL)f}{2\eta}\sqrt{\frac{2\pi\mu_o}{c}}\cos\varphi\,\frac{1}{h\sqrt{\sigma_e\left(\frac{c}{V_{ph}}\right)}}\left\{\frac{1}{\sqrt{d}}\sqrt{\frac{d/r_e}{\sin d/r_e}}\right\}e^{-\alpha' d} \qquad (1)$$

$$\times\left[e^{j\left(k_o\left(\frac{c}{V_{ph}}\right)d-\omega t+\pi/4\right)}\right]$$

where

IL	current moment
φ	angle between axis of horizontal antenna and propagation path direction
σ_e	ground conductivity at transmitter
h	effective height of ionosphere
V_{ph}	phase velocity of the only propagating mode
η	120π
r_e	earth radius
k_o	$\omega/c = 2\pi/\lambda$
d	distance between receiver and transmitter
α'	attenuation coefficient

Now there is also another magnetic field component which travels around the world along the longer segment of the same great circle path. This component at the receiver differs from equation (1) in that one only needs replace $e^{-\alpha' d}$ by $e^{-\alpha'(2\pi r_e - d)}$ and $e^{jk_o(c/V_{ph})d}$ by $e^{jk_o(c/V_{ph})(2\pi r_e - d)}$. (In addition a $\pi/2$ phase shift is introduced as this wave passes through the antipode.) The direct and the around-the-world components add to give a standing wave pattern. The positions of the standing wave minima and maxima depend on the phases of the direct and round-the-world wave components. For a realistic global ionospheric model, with local (and perhaps directional) changes in α and V_{ph} one can make the approximation

(D refers to direct wave and R the round-the-world component.)

$$(H_\varphi)_D = F\, e^{-\int_o^d \alpha_D(r)dr}\, e^{jk_o \int_o^d (c/V_{ph})_D dr} \qquad (2)$$

$$(H_\varphi)_R = F\, e^{-\int_o^{2\pi r_e - d} \alpha_R(r)dr}\, e^{jk_o \int_o^d (c/V_{ph})_R dr}\, e^{j\pi/2} \qquad (3)$$

where

$$F = \frac{ILf \cos\varphi}{2\eta h} \sqrt{\frac{2\pi\mu_o}{r_e\, c\, \sigma_e (\frac{c}{V_{ph}}) \sin\theta}}$$

$$\sin\theta = \sin\frac{d}{r_e} = \sin\left(\frac{2\pi r_e - d}{r_e}\right) .$$

The total field standing wave pattern then is the sum of the above two expressions. The main point is that if one desires to measure the parameter α_D, say by a two station measurement, it is imperative to know the phases of both $(H_\varphi)_R$ and $(H_\varphi)_D$ at both stations in order to determine receiver location with respect to the maxima and minima of the standing wave pattern. With the phases known, one still must have a reasonable estimate of $\int_o^{2\pi r_e - d} \alpha_R dr$ so that α_D can be estimated as well. It should be evident that no <u>single frequency</u>, two <u>fixed receiver measurements</u> can fix the value of α_D with any high degree of accuracy unless the other parameters are known as well. However, even if we have <u>total ignorance</u> of the values of $\int_o^{2\pi r_e - d} (\frac{c}{V_{ph}})_R dr$ and $\int_o^{d} (\frac{c}{V_{ph}})_D dr$ but some knowledge of the value of $\int_o^{2\pi r_e - d} \alpha_R dr$ one can place bounds on a range of values for α_D. (Really for $\frac{1}{d_2 - d_1} \int_{d_1}^{d_2} \alpha_D dr$.)

The uncertainty in the structure of the standing wave pattern, however, is only one element that produces an uncertainty band about α_D. The fact is that the relatively low S/N ratios encountered are responsible for estimates

of field strengths (and hence estimates of α_D) that have reasonably large confidence intervals associated with the signal level estimates. These two factors then are the prime reasons why with this limited measurement series, we can do little more than determine whether α_D is greater or less than 2.0 db/Mm.

Part II will briefly describe first the method of recording data and second the method by which the data is then processed and finally analyzed.

Part III records the data successfully recorded and analyzed and catalogs the results. In this section we will show that full potentiality of this experiment was degraded due to the high values of atmospheric noise (and as yet occasional unidentified interference in Hawaii). The experiment was originally planned for April when the atmospheric noise levels are low (about -135 dbH/$\sqrt{\text{Hz}}$). Due to delays in transmitter mitigation the higher current levels were not available until July. In July the late morning summer noise levels typically were 5 to 10 db higher than -135 dbH/$\sqrt{\text{Hz}}$. Hence the $\hat{S}/N$ ratios were reduced from 5 to 10 db from what we had originally expected. This large loss in S/N significantly increases the confidence interval (uncertainty) associated with the signal estimate.

Part IV interprets the results with regard to answering the question of how big the east-to-west attenuation coefficient is. Part V is a short summary of the principal results.

II. DESCRIPTION OF EXPERIMENTAL APPARATUS AND METHOD OF ANALYSIS

Figures 1 and 2 are simplified block diagrams showing both the field site recording apparatus and the laboratory playback facility. A significant portion of the recording apparatus was used earlier in the Lincoln wideband noise recording effort and is explained in detail elsewhere. The major changes are the following. A stable crystal oscillator (stability greater than 1 part in 10^7 per day) with its frequency generator unit provides a known signal level at a frequency less than 2 Hz away from the transmitted signal frequency. This injected signal level (known as the calibration signal) is used to calibrate the receiver up to the input of the quadrature correlation receiver for narrowband linear processing. The generator also generates all the phase references needed for the correlation receivers. The frequency stability of the crystal oscillator is checked prior to each run by comparison with the WWVL standard at Fort Collins. All of our processing reported here was done on the narrowband channel data. [A separate memo by Evans will discuss the nonlinear processing of the wideband data.] All the data was recorded on magnetic tape which were to be processed back at the Laboratory. The same equipment was used to process data from both sites at both frequencies.

The playback facility at the Laboratory is shown in Fig. 2. The data is played back with a speedup factor of 32 so as to reduce processing time from about 4 hours to several minutes. Each of the signal channels consists of a pair of quadrature correlators followed by two squarers and a summer. The outputs are then recorded on chart recorders. The units marked PAR amplifiers (Princeton Applied Research Model 120 Lock In Amplifier) consist basically of a multiplier followed by a single pole low pass filter. It can be shown that the equivalent integration time is, $T = 2(32)(RC)$. For most of our processing an $RC = 180$ sec was used which corresponds to an integration time $T \sim 3.2$ hrs. This long an integration means that each 4 hour recording period results in a single signal estimate. It should be noted that we have

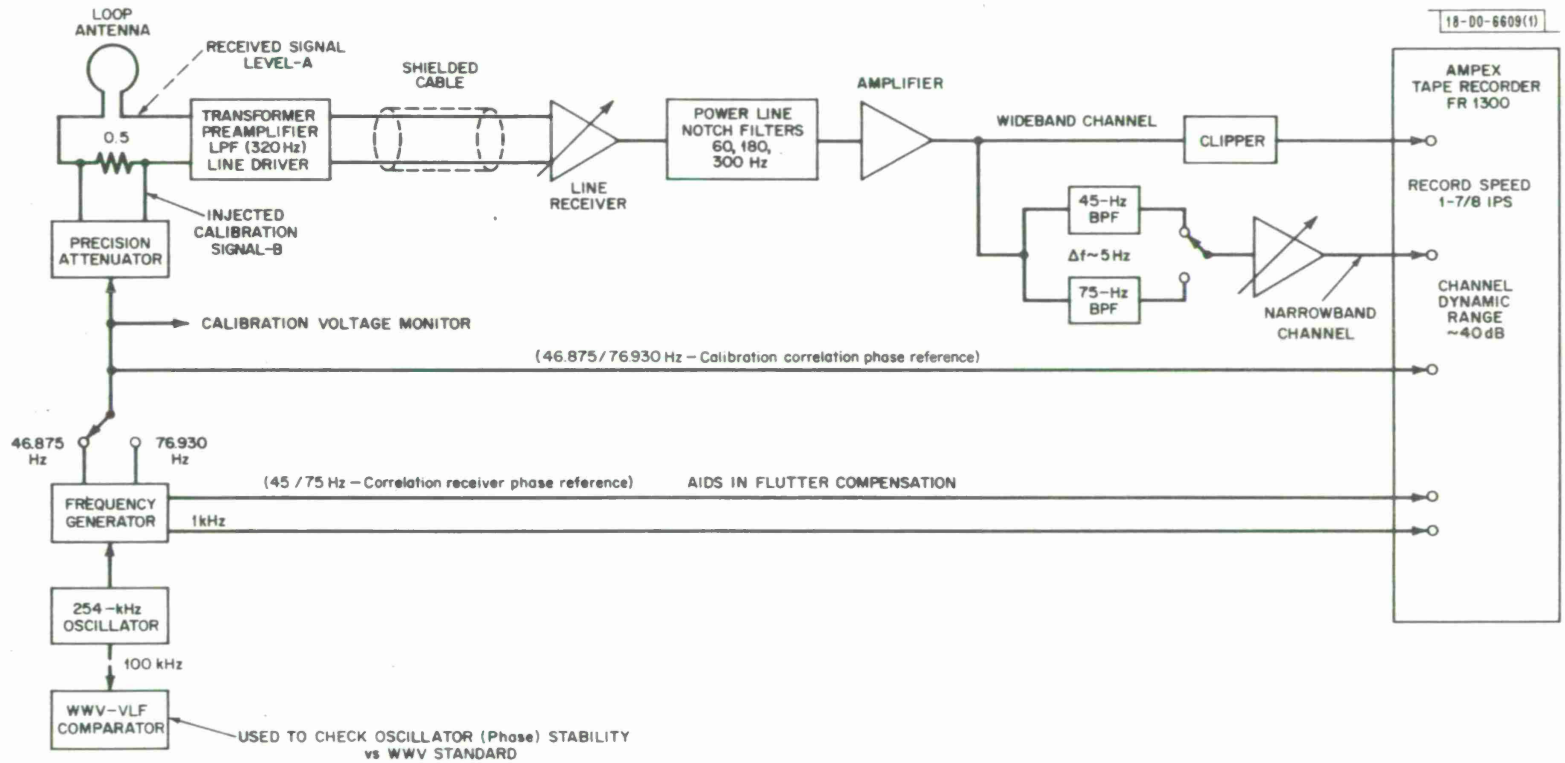

Fig. 1. Field site recording equipment.

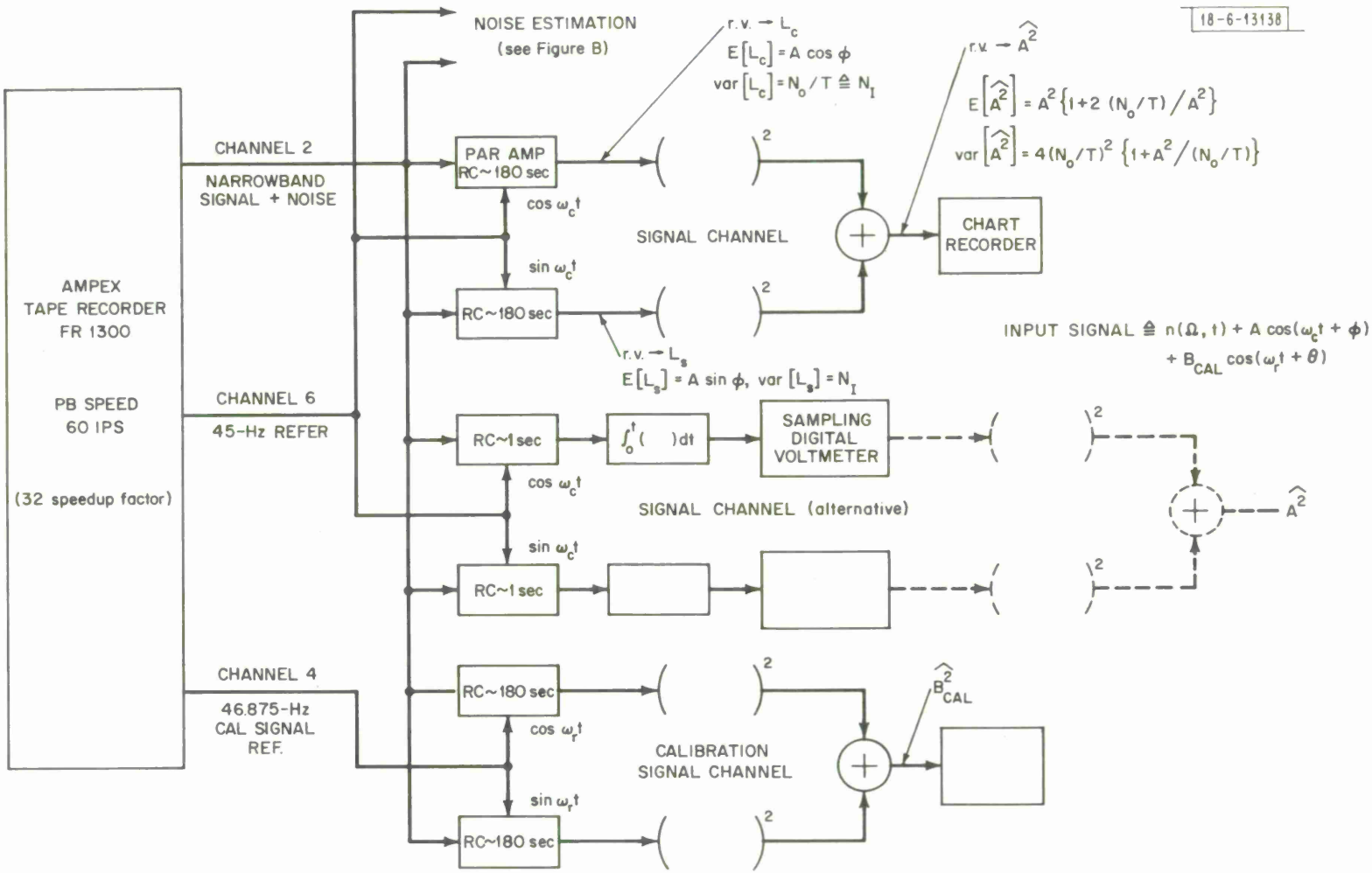

Fig. 2. Playback facility block diagram (narrowband processing).

identical receiver channels for estimation of the transmitted signal and of the injected calibration signal. With the exception of the narrowband BPF and notch filters the frequency response of the recording equipment is flat from a few Hz to about 250 Hz. Normally we try to adjust the narrowband filters so that its frequency response at the transmitter signal frequency (f_c) and at the calibration signal frequency (f_r) is identical. Thus the received signal level (A) at the output of the loop antenna is related to unbiased signal outputs (denoted by subscript c) of the summers and to the measured input calibration signal B by

$$A = B \sqrt{\frac{(\hat{A^2})_c}{(\hat{B^2})_c}} \quad . \tag{4}$$

The equivalent H_φ field is related to the antenna voltage A by

$$H_\varphi = \frac{A}{\frac{\mu \pi^2}{2} (n D^2) f}$$

$$H_\varphi = \frac{A}{(.007178) f} \tag{5}$$

where n is the number of turns in the loop and D is the diameter of the loop.

We have used on occasion an alternative configuration of the correlation receiver. The basic difference is that we have used an integrator rather than the low pass filter with the long time constant. We state, based on experience, that the appropriate configuration to use depends on the nature of the noise and in general the results are the same.

The important outputs are also shown in Fig. 2. The output of the summer is a biased estimator for A^2 (or B^2) i.e.,

$$E[\hat{A^2}] = A^2 \left\{ 1 + 2 \frac{N_o/T}{A^2} \right\} . \tag{6}$$

The point is that one must subtract off $2N_o/T$ from the sample value to get an unbiased estimate of A^2. Hence this means that N_o must be determined as well. The method of determination of N_o is discussed in Appendix A. The confidence interval associated with each measurement $\hat{A^2}$ is determined from the graph in Appendix B. The confidence interval itself is to be interpreted as a random variable and it has a certain probability $(1-\epsilon)$ of including the true value A^2.

III. DATA CATALOGUE

Due to a number of equipment malfunctions at both the Hawaii and California sites a significant percentage of the total available data was lost. Table I lists the numbers of hours of data recorded at each station. The unfortunate fact is that the number of hours in which data was recorded simultaneously at both sites amounted to only 24 hours.

Past theoretical analysis and experimental measurements provide estimates of the expected value of the field strengths at Hawaii and California. The computed values for the direct component of H_ϕ is shown in Table 2 for California and Hawaii for 45 Hz and 75 Hz (under daytime and nighttime conditions).

Tables 3 and 4 summarize the results of the measurements for California and Hawaii respectively. The column labelled "H_ϕ (dbH) - bias corrected" gives the estimates of magnetic intensity after the bias correction (see equation 6). Noise estimates which result from the variance computation (as described in appendix A) are given for three time intervals over the data record; at the beginning, in the middle and at the end of the data record. A number of noise estimates derived from the noise spectrum analysis programs are shown also. These spectra were computed from data at the tape beginning and the agreement between the two methods of noise analysis is very good for the California data (the discrepancies in the Hawaii noise evaluation methods will be discussed later in the section). The last two columns of data show the integrated noise level, N_I, and the signal to noise ratio $\hat{S}/N_I$. $\hat{S} = \hat{H}_\phi^2$ is the biased signal estimate at the summer output and N_I the integrated noise at the output of one of the quadrature correlators. We tabulate the biased signal to noise ratio rather than the unbiased signal to noise ratio because the first ratio is the one to be used in determining confidence intervals.

The factor which has seriously compromised the full potentiality of this experiment is the high noise levels along with some intermittent

TABLE 1

July

	6	7	8	9	10
Calif.	4 hrs. day	4 hrs. day	4 hrs. day 4 night	4 hrs. day 4 night	4 hrs. day 4 night
Hawaii	No Freq. Ref.	No Freq. Ref.	4 hrs. day 4 hrs. night	4 hrs. day 4 night	equip. malfunc. 4 hrs. night

45 Hz

High Current Nights

	13	14	15	16	17
Calif.	2 hrs. day	Frequency Generator Failure No Data Collected			
Hawaii	4 day 4 night	4 hrs. day	4 hrs. day	4 hrs. day	4 hrs. day

45 Hz

	20	21	22	23	24
Calif.	1 hr. day *	1 hr. day *	data tape erased at Laboratory	3 hrs. (75Hz) day	tape recorder failure
Hawaii	4 hrs. day *	4 hrs. day *	4 hrs. (75Hz) day	2 hrs. (75Hz) day data collection stopped by forest fire	

45 & 75 Hz

Summary of Available Data

California/Hawaii

All Field Strengths dbH

*Due to scheduling error receivers were set to receive 75 Hz while transmitters were at 45 Hz. As a result we have only wideband data with no frequency reference.

TABLE 2

H_φ (dbH) Estimated Field Strengths (Direct Component)

	California d = 2.52 Mm				Hawaii d = 6.53 Mm			
	45 Hz		75 Hz		45 Hz		75 Hz	
	Day	Night	Day	Night	Day	Night	Day	Night
$[10 \log \frac{\pi \mu_o}{2c} - 20 \log \eta]$	-193.34	-193.34	-193.34	-193.34	-193.34	-193.34	-193.34	-193.34
20 log IL I = 150A, L = 22.5 Km.	+130.57	+130.57	+130.57	+130.57	+130.57	+130.57	+130.57	+130.57
20 log f	33.06	33.06	37.50	37.50	33.06	33.06	37.50	37.50
20 log (cos φ) $\varphi = 22^\circ$	-.66	-.66	-.66	-.66	-.66	-.66	-.66	-.66
-10 log σ_e 1.2×10^{-4}(45 Hz), 1.7×10^{-4}(75 Hz)	39.21	39.21	37.70	37.70	39.21	39.21	37.70	37.70
-20 log h h_D = 75 km, h_N = 90 km	-97.50	-99.08	-97.50	-99.08	-97.50	-99.08	-97.50	-99.08
-10 log $(\frac{c}{V_{ph}})^*$	-1.00	-.29	-1.07	-.79	-1.00	-.29	-1.07	-.79
10 log $\frac{d/r_e}{\sin d/r_e}$	.11	.11	.11	.11	.78	.78	.78	.78
-10 log d	-64.01	-64.01	-64.01	-64.01	-68.15	-68.15	-68.15	-68.15
-αd α(45) = .75 db/Mm, α(75) = *	-1.89	-1.89	-3.25	-2.55	-4.90	-4.90	-8.42	-6.60
Total H_φ (dbH)	-155.45	-156.32	-153.95	-154.55	-161.93	-162.80	-162.59	-162.07
		-153.82 for I=200A				-160.30 for I=200A		

*$(\frac{c}{V_{ph}})$ 45 Hz, day = 1.26

$(\frac{c}{V_{ph}})$ 45 Hz, night = 1.07

} From NUSC/NLL* Measurements

$(\frac{c}{V_{ph}})$ 75 Hz, day = 1.28

$(\frac{c}{V_{ph}})$ 75 Hz, night = 1.20

α(75 Hz) day = 1.29 db/Mm, night = 1.01

* Naval Underwater Systems Center, New London Laboratory

TABLE 3

Summary of California Tapes

Date	Cal. Mon. Level (mv)	Cal Level PAR (mv)	Sig Level PAR (mv)	H_φ (dbH)	H_φ (dbH) Bias Corrected	Noise N_o from	Variance Computation	Spectral Est. (N_o)	Integrated Noise (LPF)	S/N Ratio (after integ.)	
C1 July 6 Monday (Day)	111.*	15.8 (RC=80)	1.1 (RC=80sec)	-154.8	-155.3	turn count ~ 700	-130.0 dbH/$\sqrt{Hz}$		$N_I = N_o/T$ -167.1 dbH/$\sqrt{Hz}$ @ 45 Hz	12.3	*The injected calibration system level B = (cal mon. level) x (atten. factor) where atten. factor = 7.5577×10^{-7}
C2 July 7 Tuesday (Day)	109. 106.	15.5 (180)	.88 (180)	-156.9	-157.5	264-408 694-819 1163-1273	-129.0 -127.7 -126.1	-129.4	-169.6 -168.3 -166.7	12.7 11.4 9.8	
C3 July 8 Wed. (Day)	111. 111.	15.8 (180)	1.11 (180)	-154.7	-155.0	325-555 830-925 1110-1280	-130.8 -128.3 -127.3	-130.7	-171.4 -168.9 -167.9	16.7 14.2 13.2	
C4 July 8-9 Wed. (Night)	111. 112.	16.5 (180)	.72 (180)	-158.8	-159.0	140-384 700-899 1145-1310	-134.6 -133.7 -131.9	-135.4 -134.2	-175.2 -174.3 -172.5	16.4 15.5 13.7	
C5 July 9 Thurs. (Day)	115. 112.	16.1 (180)	.87 (180)	-156.9	-157.8	270-417 680-808 1180-1290	-128.8 -126.4 -125.3		-169.4 -167.0 -165.9	12.5 10.1 9.0	
C6 (200A) July 9-10 Thurs. (Night)	113. 112.	17.2 (180)	.97 (180)	-156.6†	-156.9†	220-347 698-828 1130-1240	-130.4 -130.4 -132.0	-130.0	-171.0 -171.0 -172.6	14.4 14.4 15.9	†Current Level - 200A
C7 July 10 Friday (Day)	114. 112.	17.2 (180)	1.1 (180)	-155.4	-156.2	290-500 715-847 1110-1230	-126.4 -125.5 -124.3		-167.0 -166.1 -164.9	11.6 10.7 9.5	
C8 (200A) July 10-11 Friday (Night)	112. 111.	17.0 (180)	.73 (180)	-159.0†	-159.8†	135-420 815-1020 1200-1368	-129.1 -128.8 -129.9	-130.3	-169.7 -169.4 -170.5	10.7 10.4 11.5	†Current Level - 200A
C9 July 13 Monday (Day)	110.	17.3 (80)	.9 (80)	-157.4	-158.2	300-440 650-760	-130.8 -129.0		-167.9 -166.1	10.5 8.7	

TABLE 4
Summary of Hawaii Tapes

Date	Cal. Mon. Level (mv)	Cal Level PAR (mv)	Sig Level PAR (mv)	H_φ (dbH)	H_φ (dbH) Bias Corrected	Noise No from	Variance Computation	Spectral Est.	Integrated Noise	S/N_I (db)	
H3 July 8 Wed. (Day)	129	64	1.38	-164.1	-166.4	140-386 728-913 980-1166	-138.9 -132.3 -133.8	-136.6	$N_I = N_o/T$ dbH/$\sqrt{Hz}$ -170.9	6.8	Attenuation Factor = 7.7753×10^{-7}
H4 July 8 Wed. (Night)	127	56	1.24	-164.3	-164.9	135-382 730-925 1110-1292	-135.4 -134.4 -133.7	-137.5	-176.3	12.0	
H5 July 9 Thurs. (Day)	130	64	1.60	-162.7	-164.2	100-365 705-900 1100-1280	-132.4 -130.9 -130.7		-171.0	8.3	
H6 July 9 Thurs. (Night)	124	55	1.14	-164.7	no unbiased estimates	140-387 710-906 1195-1360	-125.7 -125.5 -127.4	-128.2†	-167.0	2.3	*Current Level - 200A †Interference present
H7 July 10 Friday (Day)	129	65				250-390 620-760 1110-1219	-127.9 -128.0 -128.5				Equipment Malfunction
H8 July 10 Friday (Night)	126	63	1.23	-165.1	-167.9*	270-410 678-800 1100-1200	-130.3 -126.8 -126.8	-133	-171.3	6.2	*Current Level - 200A
H9 July 13 Mon. (Day)	130	67	1.07	-166.6	-169.3	290-410 708-820 1250-1370	-133.8 -134.4 -129.0	-134	-172.9	6.3	
H10 July 13 Mon. (Night)	128	64	.96	-167.4	no unbiased estimates	260-420 690-810 1250-1340	-127.4 -128.6 -127.4	-126.5†	-169.6	2.2	†Interference present
H11 July 14 Tues. (Day)	128	60	.71	-169.3		208-410 717-840 1184-1270	-133.1 -135.5 -133.8		-173.6	4.3	
H12 July 14 Tues. (Night)	127	58	1.36	-163.8	-165.1	400-700 900-1200 1300-1500	-130.4 -130.4 -131.3	-134	-172.7	8.9	
H13 July 15 Wed. (Day)	132	60	2.05	-159.8	-160.5	300-500 700-900 1100-1300	-128.3 -127.2 -126.6	-132.9†	-171.2	11.4	†Interference present Huge signal estimate
H14 July 16 Thurs. (Day)	128	60	1.08	-165.8	-167.2	130-372 744-935 1128-1297	-129.6 -129.1 -128.6	-132.9†	-174.5	8.7	†Interference present
H15 July 17 Friday (Day)	127	62	.82	-168.4	no unbiased estimate	300-500 700-900 1100-1300	-128.5 -126.5 -126.5	*	-168.3	-.1	*Interference

interference at the Hawaii sites. For example the California data (Table 3) shows noise levels between -130 and -125.3 dbH/$\sqrt{\text{Hz}}$. The noise spectrum around 45 Hz is flat and no unexpected interference is present. These higher noise levels have reduced the S/N_I ratio by from 5 to 10 db lower that we would probably have observed during early spring when the experiment was originally scheduled. From Fig. B-2 in Appendix B it is obvious that reducing the S/N_I ratio from say 20 db to 10 db increases the confidence interval significantly (i.e., from about 2 db to over 8 db for $\epsilon/2 = .10$). Table 3 (for California) shows S/N_I values typically between 10 and 15 db even after integration times of 3.2 hrs. (the approximate duration of the data record being 4 hrs.). Fortunately the signal estimates, as poor as they are, are still sufficiently accurate to allow a number of positive statements to be made concerning high attenuation rates. This will be done in the next section.

The Hawaiian data is even more seriously compromised by a combination of high noise and interference. From Table 4 we see the noise varying from about -134 to -126 dbH/$\sqrt{\text{Hz}}$. For some of the data, the highest noise levels were not a result of atmospherics but resulted from some unidentified time varying and intermittent interference. It is observed that there are occasional discrepancies between the two methods of estimating noise. There are good reasons for these discrepancies. First the atmospheric spikes recorded on the wideband channels were frequently clipped due to the tape recorder's channel dynamic range limitation and hence the overall spectral level is reduced. Clipping however was not observed on the narrow band channel data which was used for the variance computation. However, the variance computation of noise is sometimes worse because the time interval over which samples are taken includes some intermittent interference whereas the shorter time interval over which the spectral estimate is derived may not include this intermittent noise. The biased signal to noise ratios are generally between 6 and 12 db with four exceptions. The exceptional cases justify further comment. Three of these days (tapes H-6, H-10 and

H-15) have exceptional high atmospheric noise such that the bias term $(2\frac{N_o}{T})$ in the signal estimator in effect masks the signal A^2. For the fourth case (tape H-11) the noise is relatively moderate ($\sim$ -134 dbH/$\sqrt{\text{Hz}}$) but the biased signal estimate itself is unusually low. Since the phase stability of the correlator phase references is known to be stable, only a few factors can result in such a low biased signal estimate (provided the transmitter has phase stability). There could be either a significant phase shift or abnormally enhanced attenuation due to some set of ionospheric conditions. Whatever the cause of this low signal value there is not yet enough additional data to support either of the above views. In all the result is that all four of these tapes have no unbiased signal estimate. The other Hawaiian data tapes do possess unbiased signal estimates with, however, unfortunately small signal to noise ratios.

IV. INTERPRETATION OF THE DATA

From equation (1) we can derive a simple expression relating the attenuation coefficient only to the direct component of the fields at California and Hawaii. Since all parameters not related to distance cancel out in the normalization it turns out that

$$\frac{(H_\varphi)_{H,D}}{(H_\varphi)_{C,D}} = \sqrt{\frac{\sin \frac{d_C}{r_e}}{\sin \frac{d_H}{r_e}}}\; e^{-\alpha'(d_H - d_C)} \qquad (7)$$

or

$$\alpha_{EW} = -.870 + \frac{[(H_\varphi)_{C,D}]_{db} - [(H_\varphi)_{H,D}]_{db}}{4.0} \quad \text{db/Mm.}$$

Originally we had planned to use the estimates of the total signal strengths at Hawaii and California in this expression and compute an effective attenuation coefficient $\tilde{\alpha}$. Since we cannot at present separate the round-the-world component from the total measured signal this effective attenuation coefficient $\tilde{\alpha}$ will be in general different from the true attenuation rate α_{EW}. However, for reasonable choices of α_{EW} and α_{WE} it can be shown that the expected range of $\tilde{\alpha}$ estimates (in the absence of significant noise) should form a reasonable band of values around α_{EW}. For example if one assumes $\alpha_{EW} = \alpha_{WE} = .7$ db/Mm it is easy to show that $\tilde{\alpha}$ will fall between .3 and 1.1 db/Mm. If experimental values of $\tilde{\alpha}$ fall in this band it is reasonable to assume that high values of $\alpha_{EW} > 2.0$ db/Mm do not exist. However as noise becomes a significant factor the expected range of $\tilde{\alpha}$ increases to the point where one cannot make any intelligent judgement of α_{EW} on the basis of the measured $\tilde{\alpha}$ values. It will be apparent that the extremely poor S/N ratios encountered in Hawaii prevent us from determining good unbiased estimates of the signal strength. Accordingly the extremely large

confidence intervals associated with these unbiased Hawaii estimators are translated into even larger confidence intervals on $\hat{\alpha}$. The point is that the Hawaii measurements turned out to be sufficiently noisy so that measurements of $\hat{\alpha}$ cannot distinguish between $\alpha_{EW} \sim .7$ and $\alpha_{EW} > 2.0$ db/Mm. For this reason no attempt has been made to compute an attenuation coefficient from simultaneous Hawaii and California measurements.

As a result of not being able to use the above simple expression for α we are forced then to compare experimental signal strengths with theoretically calculated levels (and ranges) and make some quantitative statements on the comparison. This puts us in the unfortunate circumstance of requiring reasonable knowledge of the values of h_D, h_N, $(c/V_{ph})_N$ and $(c/V_{ph})_D$. Some recent measurements at NUSC/NLL have provided us with the parameters we have used. It is not unreasonable to assume at this point that the uncertainties associated with these parameters may lead to variations in the theoretical signal levels of the order of ± 1.5 db. Even with this restriction in mind we still can make some definite statements concerning the attenuation coefficient.

It is evident from Tables 3 and 4 that the unbiased signal estimates have a considerable spread for California data as well as that for Hawaii. For each unbiased signal estimate and noise estimate a confidence interval (see Appendix C) is determined. Likewise a theoretical signal range for a particular α assumption is calculated (the range being determined by the magnitude of the standing wave uncertainty as outlined in Appendix B). The next logical step is to compare the theoretical signal range (for an assumed α) to either the confidence intervals or to some grouping of experimental unbiased signal estimates. We are going to consider two cases of interest utilizing mostly California data because of its higher S/N_I ratio.

Case a For the theoretical computations we first choose $(\alpha_{D,N})_{EW,EW} = .75$ db/Mm since this has been a commonly used value in many studies.

Case b For the theoretical computation we assume that both $(\alpha_D)_{EW}$ and $(\alpha_N)_{EW}$ are greater than 2 db/Mm. For the west to east direction we assume $(\alpha_{D,N})_{WE} = .75$ db/Mm.

Figure 3 shows both the biased and unbiased signal estimates as well as the confidence intervals for each biased experimental signal estimate.

Table 5 lists the theoretical range of signal values for cases a and b. The first row lists the values of computed field strength of the direct component only (values taken from Table 2). The second row lists a weighted experimental average of the unbiased signal estimators $(H_\varphi^2)_{u,i}$ of the total signal where

$$\overline{(H_\varphi^2)_u} = \frac{\sum_{i=1}^{M} \left[\frac{(H_\varphi^2)_u}{N_I}\right]_i}{\sum_{i=1}^{M} \frac{1}{(N_I)_i}} \quad . \tag{8}$$

The difference between the theoretical estimate and the composite experimental values are listed in row 3. The difference under California daytime conditions is only 0.8 db/Mm, suggesting compatibility between experimental and theoretical results (for case a). The other columns show considerably larger differences which will be discussed later in this section. The range of theoretical values in row 4 are indicated on Fig. 3 as solid vertical bars. It can be easily seen that the primary effect of increasing or decreasing the east to west attenuation coefficient, $(\alpha_{D,N})_{EW}$, is just to shift the solid vertical bars up or down respectively. (The change in the length of the solid bars being a secondary effect.) One now should compare the unbiased signal estimates to the theoretical range of total signal strength (for a particular α).

For the daytime California results none of the unbiased signal estimates

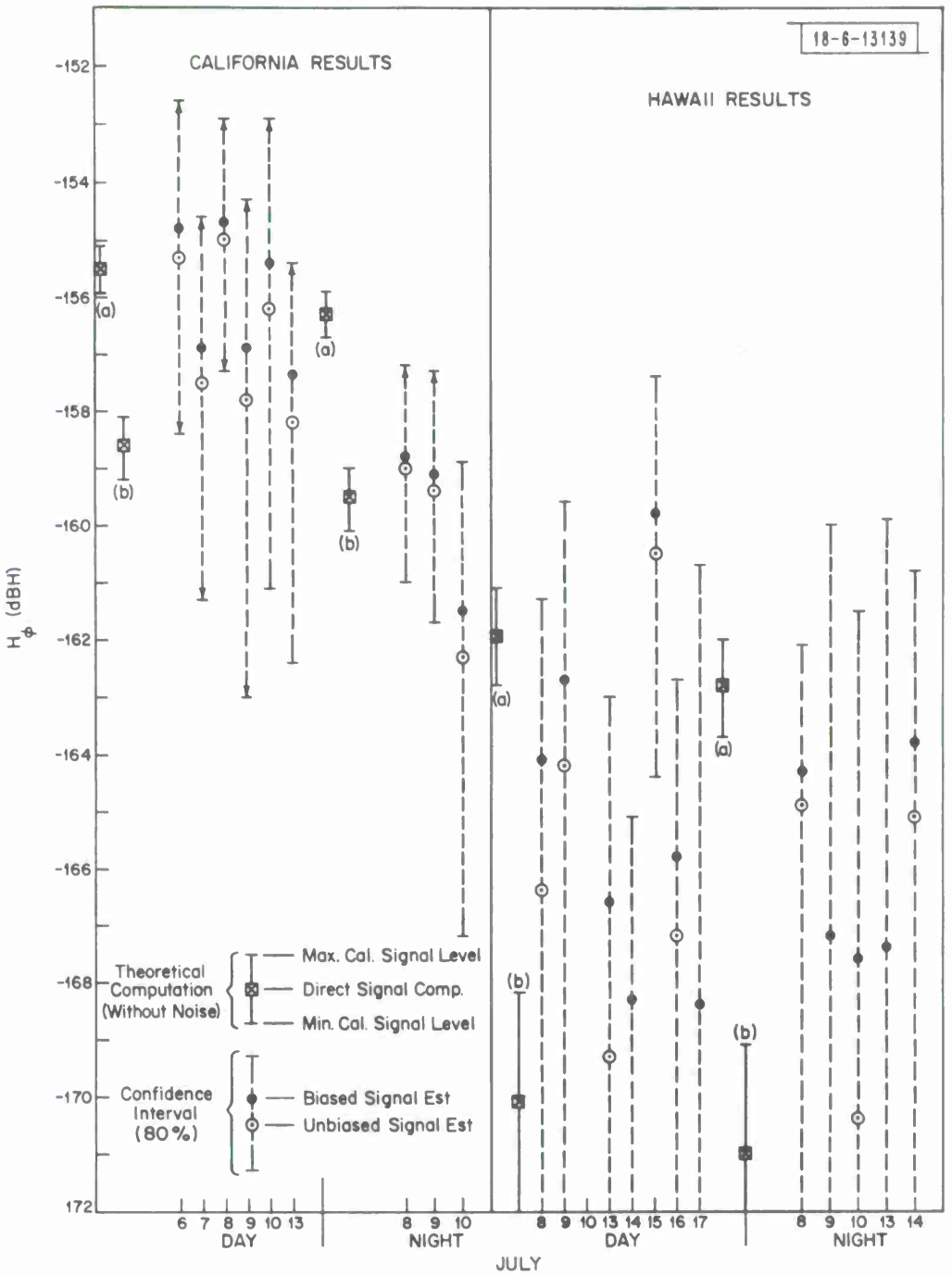

Fig. 3. Confidence intervals (California - Hawaii results).

TABLE 5

Theoretical Computations

Case a $(\alpha_{D,N})_{EW,WE}$ = .75 db/Mm I = 150A f = 45 Hz

		California		Hawaii	
		Day	Night	Day	Night
1.	H_ϕ - Direct Component (see table 2) (Theoretical Estimate)	-155.5 dbH	-156.3 dbH	-161.9 dbH	-162.8 dbH
2.	$(H_\phi^2)_u$ - Composite Experimentally Measured Value (Unbiased)	-156.3 dbH	-159.5		
3.	Difference = (Theor. Est. - Composite Exp. Est.)	+0.8 db	+3.2 db		
4.	Range of calculated signals due to standing wave pattern interference $\lvert(H_\phi)_T\rvert_{max}$ & $\lvert(H_\phi)_T\rvert_{min}$.	Max. -155.1 Min. -155.9	-155.9 -156.7	-161.1 -162.8	-162.0 -163.7

Case b $(\alpha_{D,N})_{EW}$ = 2.0 db/Mm, $(\alpha_{D,N})_{WE}$ = .75 db/Mm

		California		Hawaii	
		Day	Night	Day	Night
1.	Direct Comp. (Theoretical Est.)	-158.6 dbH	-159.5	-170.1	-171.0
4.	Range of total signal due to standing wave interference.	Max. -158.1 Min. -159.2	-159.0 -160.1	-168.2 -172.6	-169.1 -173.5

fall below the lower limit of range for $(\alpha_D)_{EW}$ = 2.0 db/Mm. This suggests that during daytime conditions east to west attenuation rates are smaller than 2.0 db/Mm. Since all the confidence intervals include the theoretical signal range for $(\alpha_D)_{EW}$ = .75 db/Mm it is possible that the attenuation value is in fact the true value, although the grouping of the unbiased sample estimates suggest it may be somewhat higher. The likelihood that $(\alpha_D)_{EW}$ < .75 db/Mm also seems less feasible when one considers that the composite weighted unbiased signal estimate is about -156.3 db/Mm.

For the nighttime California measurements, all three unbiased estimates fall considerably lower than the signal levels expected for $(\alpha_N)_{EW}$ = .75 db/Mm (in fact the unbiased estimates group reasonably close to the signal levels expected for $(\alpha_N)_{EW}$ = 2.0 db/Mm). In addition the upper limits of the confidence intervals do not reach the minimum theoretical signal level for $(\alpha_N)_{EW}$ = .75 db/Mm. One must however be very careful not to jump to the conclusion that $(\alpha_N)_{EW}$ is in fact nearly 2.0 db/Mm. It must be realized that the theoretical signal strengths were derived on the basis of values of h and c/V_{ph} as given by Table 2. It may be possible that h_N might be as large as 95km and $(c/V_{ph})_N$ as large as 1.2.* These values would lower all the theoretical signal levels (at night) by about 1.3 db. Even in this case a composite unbiased signal estimate for California would indicate an attenuation coefficient closer to 1.5 db/Mm rather than .75 db/Mm. The nighttime data seems then to indicate an attenuation coefficient $(\alpha_N)_{EW}$ somewhere between .75 db and 2.0 db with a reasonable probability that the value might be towards the larger value.

One can strengthen the above arguments by examining the weighted average (composite) signal strengths and the composite confidence intervals associated with these averages. The computation of these composite confidence intervals is shown in Appendix D. Figure 4 shows the daytime

*The two values taken together are inconsistent with recent NUSC/NLL measurements (which indicate the values used in Table 2 are more appropriate). Most theoretical estimates for $(c/V_{ph})_N$ are between 1.1 and 1.2.

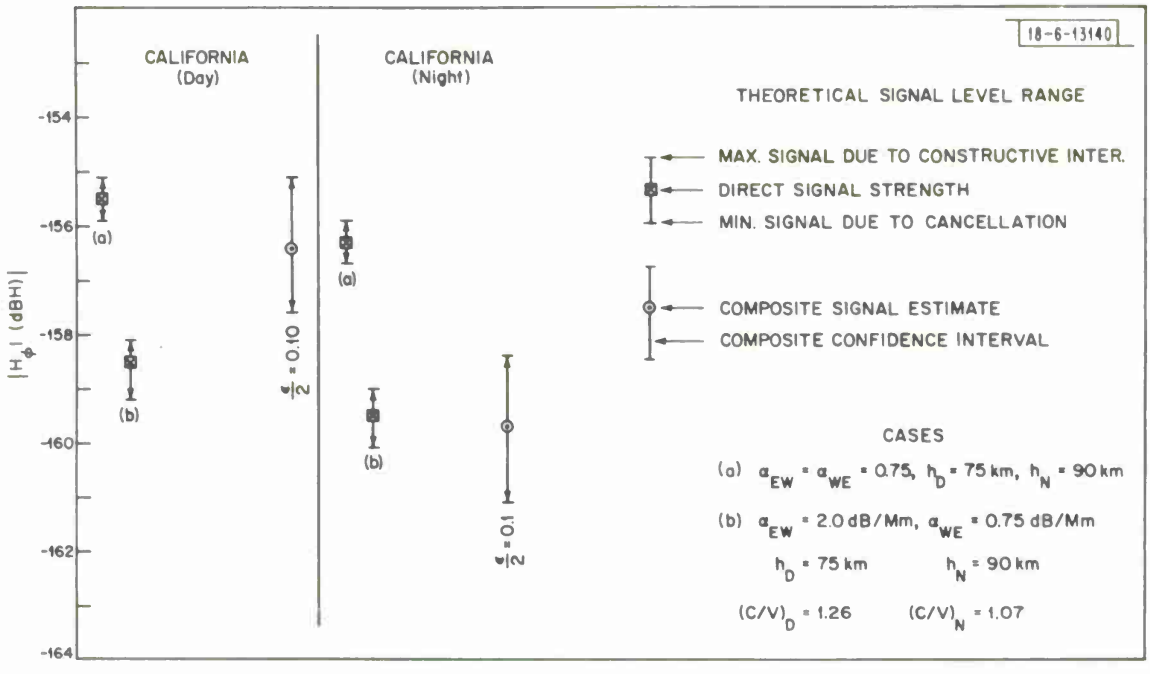

Fig. 4. Composite confidence intervals.

and nighttime composite unbiased signal estimates and the associated confidence limits (for $1-\epsilon = .80$) along with the theoretical signal ranges for $\alpha_{EW} = .75$ db/Mm and 2.0 db/Mm. It is immediately obvious that under daytime conditions the confidence limit includes the range of values for $\alpha_{EW} = .75$ db/Mm and excludes those for $\alpha_{EW} \geq 2.0$ db/Mm. It is safe to state that there is less than a 10% probability that the true value of α_{EW} is 2.0 db/Mm or greater. It is also apparent that at night the range of signal values for $\alpha = .75$ db/Mm are well above the composite confidence limit. By making other less reasonable choices for h, (c/V_{ph}) and σ_e it is still difficult to bring the range down to the upper limit of the confidence interval. This is the basis for believing that the nighttime attenuation rate is significantly larger than .75 db/Mm.

The data from Hawaii to a degree support (or at least does not reject) the conclusions reached by use of the California data alone. The confidence intervals are however so large that they cover both the signal range for $\alpha = .75$ db/Mm and 2.0 db/Mm. The exceptions are the daytime measurements on July 13 and 14 where the confidence intervals are below the signal range for $\alpha = .75$ db/Mm. These points would seem to indicate that the daytime attenuation rate was also somewhat greater than .75 db/Mm. The grouping of the unbiased signal estimates is so spread out that any estimate of the probable attenuation rate range is premature. The confidence intervals for both the day and nighttime data seem to indicate that $(\alpha_{D,N})_{EW} > .75$ db/Mm.

Since we have integrated over such a long period (usually about 3 to 4 hours) the possibility arises that a relative phase shift between the signal phase and the internally generated reference phase may occur during this extended period. The result of this would be a signal estimate lower than the true signal level by an amount which depends on the degree of the phase shift. It should be emphasized that great effort was taken to routinely check the receivers phase stability. Observations during the playback of the data tapes revealed no phase shifts due to the receiver malfunctions. Accordingly if a signal phase shift occurred it must be due to changing ionospheric

conditions. Since we have operated only when the entire propagation path was entirely in daytime conditions or in nighttime conditions, one expects the phase shift due to changing ionospheric conditions to be very small and to effect the signal estimate to a negligible degree.

Up to the present time we do not have sufficiently high antenna currents to determine whether such ionospheric phase shifts do occur. It should be mentioned that analysis of the California data did not reveal any abrupt ionospheric induced phase shift over that part of the path. With the present signal levels one cannot test whether there is a gradual phase shift of the signal phase due to changing ionospheric conditions.

V. SUMMARY

The following list of observations is a summary of both our field experiences and analysis of the data.

1. There is ample evidence that attenuation rates (at 45 Hz) are less than 2.0 db/Mm for propagation over paths entirely under daytime conditions, i.e., $(\alpha_D)_{EW} < 2.0$ db/Mm.

2. The best guess is that the daytime attenuation coefficient, $(\alpha_D)_{EW}$, is between .75 and 1.2 db/Mm if the choices used for h, σ_e and c/V_{ph} are the correct ones.

3. At night there appears to be a substantially lower than expected signal level. The best guess is that the attenuation coefficient is somewhere between 1.2 and 1.8 db/Mm. The S/N ratios for these data (in California) are high so that we have high confidence that these points are quite accurate signal estimates. This higher than expected attenuation rate, $(\alpha_N)_{EW}$, is the major surprise of the entire experiment.

4. To improve upon the results of this experiment a number of factors can be considered. The biggest improvement would be to make the same set of measurements at a less noisy period (the winter season). This should increase the signal to noise ratio by some 5 to 10 db. A larger current level say 300A will raise the signal by 6 db. It is doubtful that integrating over periods exceeding 5 hrs. will be possible since one wants to keep well away from sunrise and sunset periods at Wisconsin and Hawaii (about a 2 db improvement). Hence one can get roughly a 13 to 18 db increase in S/N ratio with the above. Then if the round-the-world contribution can be separated from the total signal, the signal to noise improvement will result in much better estimates of α (a report is in preparation on future ELF propagation measurements).

APPENDIX A NOISE INTENSITY MEASUREMENTS

Accurate knowledge of the noise intensity (at the signal frequency) is necessary for the following two reasons.

1. The estimate of the signal power at the output of the receiver's summer is a biased estimator (i.e., $E[\hat{A^2}] = A^2 + 2(\frac{N_o}{T})$). The bias consequently must be subtracted from the sample value $\hat{A^2}$ to give the unbiased estimate of A^2.

2. The confidence limits on each estimate $\hat{A^2}$ depend on the ratio $\frac{\hat{A^2}}{N_I}$ (where $N_I = \frac{N_o}{T}$). Accordingly a small confidence interval for $\hat{A^2}$ requires an even smaller confidence interval for N_I.

For purposes of this experiment we have set an acceptable confidence interval of $\pm .2$ db on N_I. It should be noted that the best way to reduce the confidence interval in estimating a signal level is to integrate over the entire data record and come up with a single value A^2. On the other hand, to reduce the confidence interval in noise intensity estimation the scheme is to get as many independent samples in the data record as possible. We will defer until the end of this section, the method which selects the number of samples needed to provide a specified confidence interval about N_I.

Figure A-1 shows the primary method by which the noise intensity N_o' was computed. The output of a single correlator (PAR) is sampled at a reasonable high rate f_{sample} (~ 40/sec) and recorded on magnetic tape. The output random variable is denoted as L_x (x denotes either the cosine or sine reference channel). The sample mean $\overline{m_x}$ and sample variance $\overline{\sigma_x^2}$ are defined by

$$\overline{m_x} = \frac{1}{N} \sum_{i=1}^{N} (L_x)_i \qquad (a-1)$$

$$\overline{\sigma_x^2} = \frac{1}{N-1} \sum_{i=1}^{N} \{(L_x)_i - \overline{m_x}\}^2 \quad . \qquad (a-2)$$

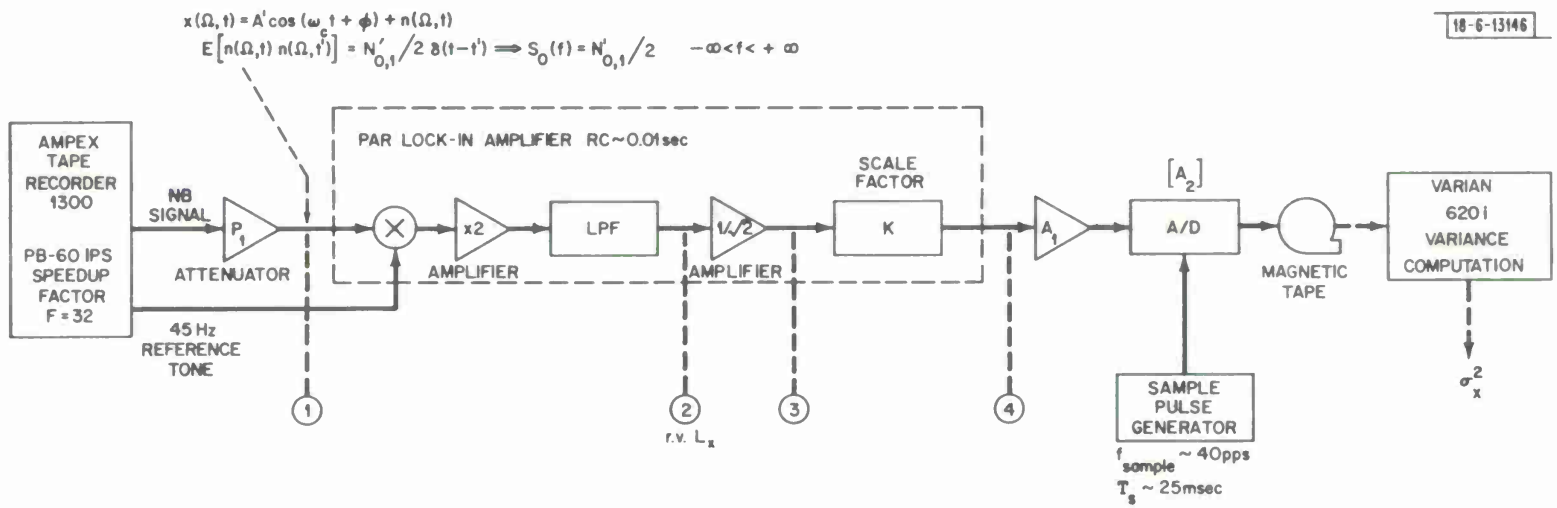

Fig. A-1. Primary noise estimation method.

It can be shown $E[\overline{m}_c] = A \cos \varphi$, $E[\overline{m}_s] = A \sin \varphi$ and

$$E[\overline{\sigma_x^2}] = \text{var}\,[L_x] = \text{var}\,[L_s] = \text{var}\,[L_c] = \frac{N_o}{T} \qquad (a\text{-}3)$$

where $T = 2(32)RC$. (RC being the time constant of the LPF.) The above is true provided the random variables $(L_x)_i$ are identically distributed and statistically independent. [In the analysis of the California - Hawaii data in general there was observed a significant general increase in noise intensity from the beginning of the data record to the end. Thus we were forced to compute the variance over shorter intervals when the total noise level was relatively constant so as to make the $(L_x)_i$ reasonably identically distributed. Values of the computed noise intensity at the beginning, middle and near the end of the tape are shown in tables 3 & 4 in Section III.]

The important point is that the sample variance is computed from the N independent outputs of one of the correlators. We use $(\overline{\sigma_x^2})_2$ as an estimator for $\frac{N_{o,1}}{T}$ from which we can then compute the estimate of $N_{o,1}$. The details of these computations will be outlined in the next few paragraphs. $N_{0,1}$ (as well as H_N $(dbH/\sqrt{Hz})$) will be interpreted as the double sided noise intensity (i.e., $S(f) = \frac{N_{o,1}}{2}$, $-\infty < f < +\infty$). Mean and variance computer programs are available for the Varian 620i.

Since the received signal levels are given in terms of an H field at the input to the antenna, we will also find an equivalent input H_N noise intensity field from the Varian computed variance. Let us work backwards from the Varian computed variance $\overline{\sigma_x^2}$. The variance at station 4 in Fig. A-1 is then given by

$$(\overline{\sigma_x^2})_4 = \frac{1}{(A_1 A_2)^2}\ \overline{\sigma_x^2} \ . \qquad (a\text{-}4)$$

There is a scale factor K in the PAR so that (K being different for every sensitivity scale)

$$\overline{(\sigma_x^2)}_3 = \frac{1}{(K)^2} \overline{(\sigma_x^2)}_4 . \qquad (a-5)$$

The next step is to relate the output at station 3 to the input at station 1. The input noise at station 1 is characterized by white noise such that

$$E[n_1(\Omega, t) n_1(\Omega, t')] = \frac{N_{o,1}}{2} \delta(t-t') . \qquad (a-6)$$

The output noise at station 3 can be shown to be related by

$$\overline{(\sigma_x^2)}_3 = \underbrace{(\tfrac{1}{2})}_{\substack{\text{single quad} \\ \text{component}}} \times \underbrace{(2)^2}_{\substack{\text{normalization} \\ \text{factor}}} \times \underbrace{(\frac{N_{o,1}}{2} \cdot \frac{1}{2RC})}_{\text{effect of LPF}}$$

$$\times \underbrace{(\frac{1}{\sqrt{2}})^2}_{\substack{\text{meter scale} \\ \text{factor}}}$$

$$\overline{(\sigma_x^2)}_3 = \frac{N_{o,1}}{4RC} = \frac{N_{o,1}}{2} \frac{1}{T} . \qquad (a-7)$$

For the tape recorder contribution there is both a question of amplification and the expansion of bandwidth due to playback speedup. The amplification factor will be accounted for in the calibration process. The effect of speedup is to increase the noise bandwidth by the speedup factor F. The noise intensity in record time is related to noise intensity in playback time by F. The system gain from the antenna output to the tape recorder output is determined from the calibration process

$$G_{sys} = \frac{\sqrt{\hat{B}_\epsilon^2}}{B} = \frac{\text{rms value of the cal. level measured at the PAR input}}{\text{rms value of cal. level at injection point.}}$$

Following the tape recorder we have been using an attenuator (with gain $P_1 < 1$). Thus the noise intensity at the antenna output is related to the noise

intensity at the attenuator output by

$$N_{o,ant} = N_{o,1} \frac{1}{(G_{sys} P_1)^2} \cdot F \quad . \tag{a-8}$$

Finally the noise at the antenna output (in volts) is related to an equivalent magnetic field noise intensity by

$$H_N = \frac{\sqrt{N_{o,ant}}}{(.007178)f} \quad . \tag{a-9}$$

Equations a-4, a-5, a-7, a-8 and a-9 are combined to yield

$$H_N^2 = \frac{1}{(.007178\,f)^2} \frac{F}{(G_{sys} P_1)^2} (4RC) \frac{1}{K^2} \frac{1}{(A_1 A_2)^2} \overline{\sigma_x^2}^* \tag{a-10}$$

It should be noted that H_N is also in rms units because of the $1/\sqrt{2}$ factor in the PAR unit. The results of this noise measurement are listed in tables 3 and 4 in Section III under the column 'noise from variance computation'.

The virtue of the above noise analysis is that a number of noise estimates for each tape takes only several minutes after the equipment has been set up and calibrated. There is an alternative method of computed noise intensity which we have used on occasion. The method consists of digitizing large segments of the wideband channel on playback. The resulting digital tape will be in the same format as was used for Lincoln's wideband noise study. One of the spectral programs produces a noise spectrum from which one can pick off the noise intensity level at 45 Hz. The primary disadvantage of this method is that it is time consuming and costly in computer time. Again on table 3 we have several spectral estimates made near the beginning of the tape. The close agreement between the noise intensity made by variance computation and that made by the spectrum estimate is extremely close. The advantage of the spectrum computation is that it shows clearly

*For the actual analysis the following constants were used $A_1 = A_2 = 1$, RC = .01 sec, F = 32, $P_1 = \frac{1}{10}$ and $K = (10/(50 \times 10^{-3}))$.

sources of interference at frequencies sufficiently close to 45 Hz (75 Hz) which may affect the signal estimate. A memo by Evans[7] will show a number of spectra for Hawaii which exhibit local interference which has degraded some of the data.

As a slight digression we will outline how we select the number of samples needed to satisfy a specified confidence interval about $\hat{H}_N$ (dbH). Let us first assume that the output of the correlator $(L_x)_i$ has had its mean subtracted off. Denote this new variable by ℓ_i. For real time integration times of the order of .1 sec or greater; previous wideband noise studies indicated that this variable has a normal distribution. In particular

$$f_{\ell_i}(\ell_i) = \frac{1}{\sqrt{2\pi}\sqrt{\frac{N_{o,1}}{T}}} \; e^{-\frac{\ell_i^2}{2}\left(\frac{N_{o,1}}{T}\right)^{-1}} \qquad \text{(a-11)}$$

The variance in this case is computed from

$$\hat{\sigma}^2 = \frac{1}{N}\sum_{i=1}^{N} \ell_i^2 \triangleq \frac{1}{N}\chi^2$$

$\hat{\sigma}^2$ itself is then a random variable with a distribution which can be shown to be a χ^2 distribution with N degrees of freedom i.e.,

$$f_{\hat{\sigma}^2}(\hat{\sigma}^2) = N f_{\chi^2}(N\hat{\sigma}^2).$$

Hence it can be shown

$$f_{\hat{\sigma}^2}(\hat{\sigma}^2) = \frac{N}{(N_{o,1}/T)}\; 2^{N/2}\,\Gamma\left(\frac{N}{2}\right)\left\{N\frac{\hat{\sigma}^2}{(N_{o,1}/T)}\right\}^{\frac{N}{2}-1} \times e^{-\frac{N\hat{\sigma}^2}{(N_{o,1}/T)}} \quad \text{for } \hat{\sigma}^2 \geq 0$$
$$= 0 \quad \text{for} \quad \hat{\sigma}^2 < 0 \qquad \text{(a-12)}$$

The mean and variance of the random variable $\hat{\sigma^2}$ are most easily found by determining the moment generating function for the random variable ℓ_i^2. This can be shown to be

$$\psi_{\ell_i^2}(t) = \frac{1}{\sqrt{2\left(\frac{N_{o,1}}{T}\right)}\ \sqrt{\frac{1}{2\left(\frac{N_{o,1}}{T}\right)} - t}}$$

For independent random variables we have (define $Z = \Sigma \ell_i^2$)

$$\psi_Z(t) = \psi_{\Sigma \ell_i^2}(t) = \prod_{i=1}^{N} \psi_{\ell_i^2}(t)$$

$$\psi_Z(t) = \frac{1}{\left(2\frac{N_{o,1}}{T}\right)^{N/2} \left\{\frac{1}{2\left(\frac{N_{o,1}}{T}\right)} - t\right\}^{N/2}} \quad . \tag{a-13}$$

Now the first two moments of the distribution are found from equation a-13

$$E[\hat{\sigma^2}] = \frac{1}{N} E[Z] = \frac{1}{N} \frac{\partial \psi_Z(t)}{\partial t}\Big|_{t=0}$$

and

$$\text{var}[\hat{\sigma^2}] = \frac{1}{N^2}\{E[Z^2] - (E[Z])^2\} = \frac{1}{N^2}\left\{\frac{\partial^2 \psi_Z}{\partial t^2}\Big|_{t=0} - \left(\frac{\partial \psi_Z}{\partial t}\Big|_{t=0}\right)^2\right\}.$$

It is easy then to show

$$E[\hat{\sigma^2}] = \left(\frac{N_{o,1}}{T}\right) \text{ and} \tag{a-14}$$

$$\text{var}[\hat{\sigma^2}] = \frac{2\left(\frac{N_{o,1}}{T}\right)^2}{N} \quad . \tag{a-15}$$

From a-14 one sees that $\hat{\sigma^2}$ is an estimator of $\frac{N_{o,1}}{T}$ and from a-15 the variance of the estimate decreases inversely with the number of samples chosen.

It is observed that $f_{\hat{\sigma}^2}(.)$ is a function both of N and the true variance $(\frac{N_o, 1}{T})$. The confidence limits σ_U^2 and σ_L^2 are chosen such that

$$\int_{\sigma_U^2}^{+\infty} f_{\hat{\sigma}^2}(\hat{\sigma}^2; N, \frac{N_o, 1}{T})\, d\hat{\sigma}^2 = \frac{\epsilon}{2} \qquad (a-16)$$

and

$$\int_{o}^{\sigma_L^2} f_{\hat{\sigma}^2}(\hat{\sigma}^2; N, \frac{N_o, 1}{T})\, d\hat{\sigma}^2 = \frac{\epsilon}{2} . \qquad (a-17)$$

It should be clear that both σ_L^2 and σ_U^2 are functions of both ϵ and N. For large values of N, Holsinger[6] provides some approximate formulas for the confidence interval

$$\sigma_U^2 = \hat{\sigma}^2 \left[1 - \frac{K_\epsilon}{\sqrt{2(N-1)}}\right]^{-2}$$

$$\sigma_L^2 = \hat{\sigma}^2 \left[1 + \frac{K_\epsilon}{\sqrt{2(N-1)}}\right]^{-2}$$

where K_ϵ is defined by

$$\frac{\epsilon}{2} = \frac{1}{\sqrt{2\pi}} \int_{K_\epsilon}^{\infty} e^{t^2/2}\, dt .$$

Thus for a value $\frac{\epsilon}{2} = 10\%$ and for a $\pm .2$ db interval, one requires of the order of 1,600 samples. With a sample interval of 25 msec and for 1 minute of playback data some 2400 samples are normally collected for the variance computation.

APPENDIX B CONFIDENCE INTERVAL FOR SIGNAL ESTIMATES

The output of the typical receiver structure shown in Fig. 2 is the random variable A^2 where

$$A^2 = L_c^2 + L_s^2 \,. \tag{b-1}$$

The random variables $L_c(\Omega, t)$ and $L_s(\Omega, t)$ are assumed to be statistically independent and normally distributed with identical known variances but with different means. The probability density functions are therefore

$$f_{L_c}(L_c) = \frac{1}{\sqrt{2\pi N_I}} \, e^{-\frac{(L_c - A\cos\varphi)^2}{2N_I}} \tag{b-2}$$

and

$$f_{L_s}(L_s) = \frac{1}{\sqrt{2\pi N_I}} \, e^{-\frac{(L_s - A\sin\varphi)^2}{2N_I}} \,.$$

It is easy to show (see Van Trees [7]) that the cumulative distribution function for A^2 is related to the Marcum Q function by

$$P(A^2 \le \gamma^2) = 1 - \int_{\gamma/\sqrt{N_I}}^{\infty} \ell \, I_o(a\ell) \, e^{-\frac{\ell^2 + a^2}{2}} \, d\ell \tag{b-3}$$

$$P(A^2 \le \gamma^2) \triangleq 1 - Q\left(\frac{A}{\sqrt{N_I}}, \frac{\gamma}{\sqrt{N_I}}\right) \tag{b-4}$$

where

$$\ell = \sqrt{\frac{A^2}{N_I}} \quad \text{and} \quad a = \sqrt{\frac{A}{N_I}} \,.$$

Let us select a confidence level ϵ. It is standard practice to derive the confidence curves from the relations

$$\frac{\epsilon}{2} = P(\hat{A^2} \leq \gamma^2_L) \qquad (b\text{-}5)$$

and

$$\frac{\epsilon}{2} = P(\hat{A^2} \geq \gamma^2_H) \quad .$$

Figure B-1 shows Marcum's Q function with the curve parameter $\frac{A}{\sqrt{N_I}}$ converted to db. Figure B-2 shows the confidence curves (for fixed levels of ϵ) which are derived from equations b-4 and b-5 and Fig. B-1. Using the confidence curves is particularly simple. Assume the confidence level ϵ is specified and that one measures a value $\hat{A^2}/N_I$. A horizontal line is drawn on Fig. B-2 through this value of $\hat{A^2}/N_I$. The two values of A^2/N_I [defined by the intersection of the horizontal line with the confidence curves (with parameter $\epsilon/2$)] form the limits of the confidence interval. An example of how to construct a confidence interval is also shown on the figure. The confidence interval $(A_L^2/N_I, A_H^2/N_I)$ is itself a random variable. The true value of A^2/N_I is included within this interval with probability $1-\epsilon$. From these confidence curves it is easy to see that the confidence interval rapidly increases in size with decreasing values of $\hat{A^2}/N_I$.

We also use on occasion the term confidence band. To determine a confidence band one first computes a theoretical signal level and the corresponding signal to integrated noise ratio. Then a vertical line is drawn on Fig. B-2 through the value of S/N_I intersecting the appropriate pair of confidence curves at two points. The range of expected sample $\hat{S}/N_I$ values enclosed by two horizontal lines through the two intercept points will be called the confidence band. In brief the difference between the confidence band and the confidence interval is the following. If we have a theoretically calculated signal value, then the confidence band gives the range of sample biased signal levels that one might experimentally measure {$(1-\epsilon)100\%$ of the samples would be in the band} provided that the theoretical calculated value were in fact the true value. If on the other hand we are presented with a set of experimentally measured biased signal levels then for each of these measure-

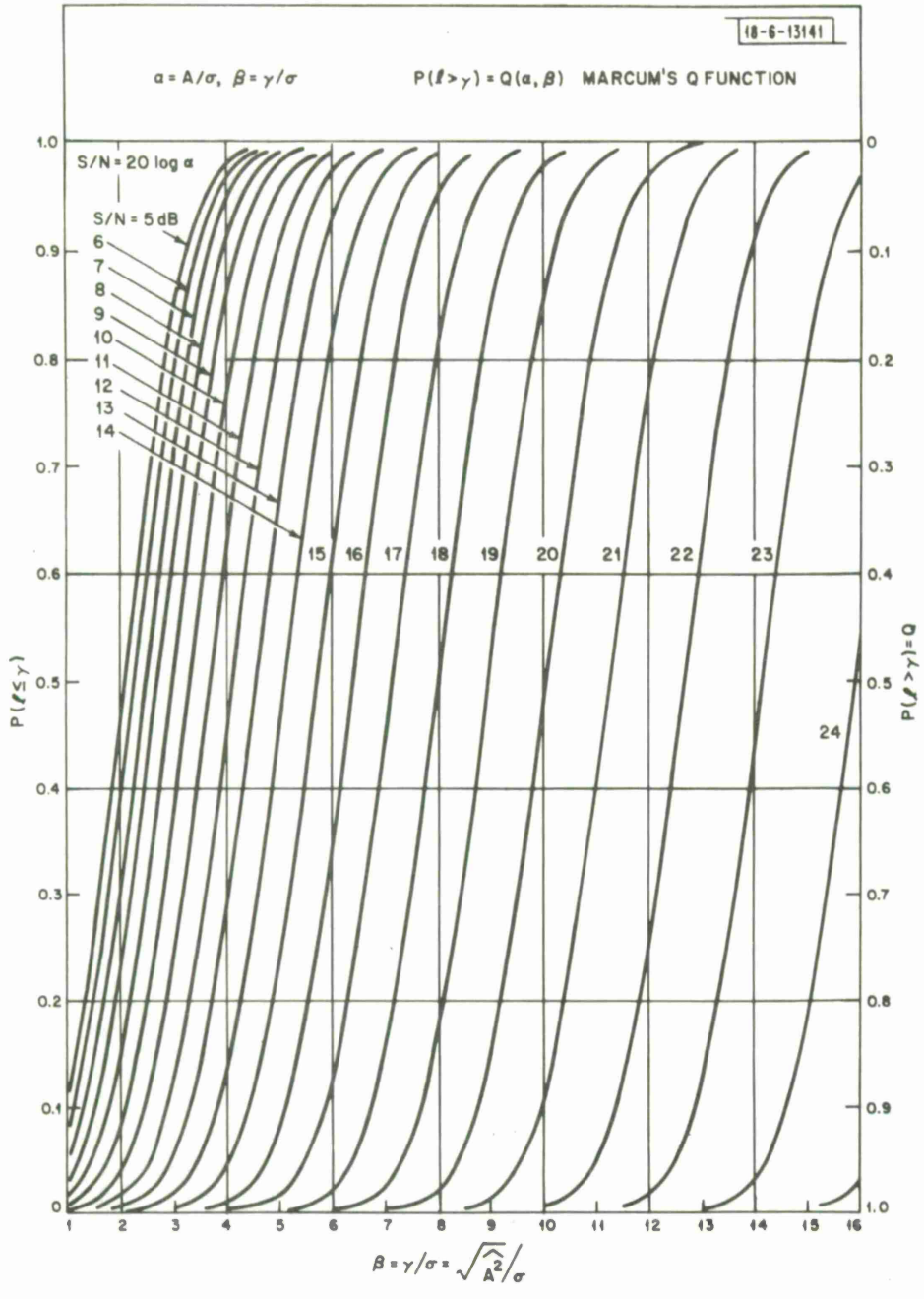

Fig. B-1. Cumulative probability distribution (Marcum's Q function).

ments we have a unique confidence interval. The statement can then be made that with probability $(1-\epsilon)100\%$ each interval will include the true value of signal (or rather the true value of S_{true}/N_I).

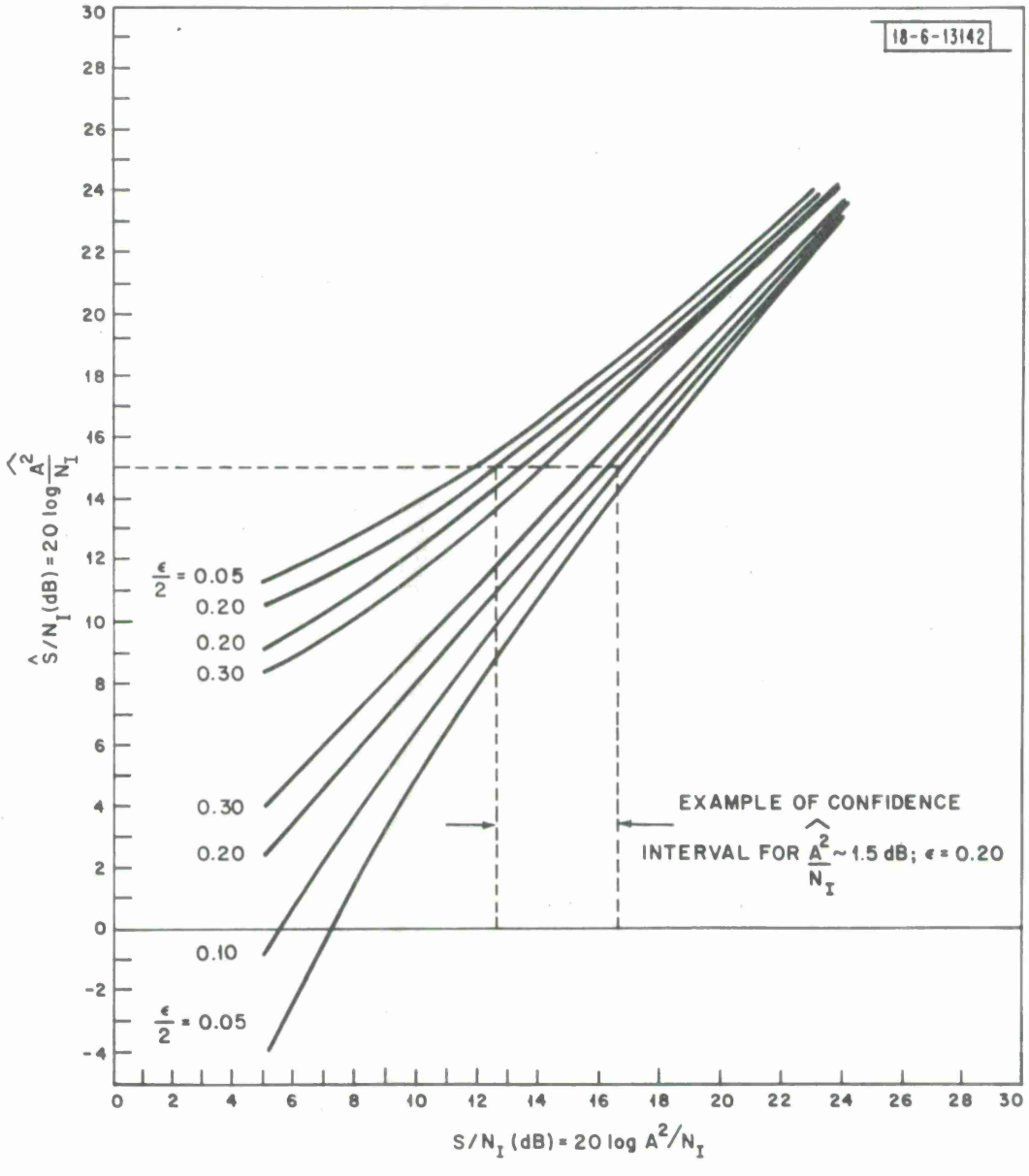

Fig. B-2. Confidence curves (for Marcum's Q function).

APPENDIX C ESTIMATES OF THE EFFECTS OF THE ROUND-THE-WORLD WAVE

It is now apparent that the earth-ionosphere cavity can have a standing wave field pattern with significant nulls and peaks provided that the attenuation rate (in at least one direction) is small. This is normally the case for propagation in the lower ELF domain. Under the conditions of a world-wide isotropic and homogeneous ionosphere of constant height, the total field may be decomposed into a direct component and an around-the-world component given by

$$\frac{(H_\varphi)_D}{F_D} = e^{-\alpha' d}\, e^{jk_o \frac{c}{V_{ph}} d} \qquad (c\text{-}1)$$

and

$$\frac{(H_\varphi)_R}{F_R} = e^{-\alpha'(2\pi r_e - d)}\, e^{jk_o \frac{c}{V_{ph}}(2\pi r_e - d)}\, e^{j\pi/2} \qquad (c\text{-}2)$$

where

$$F_D = F_R = \frac{ILf}{2\eta h} \cos\omega \sqrt{\frac{2\pi\mu_o}{r_e c \sigma_e (\frac{c}{V_{ph}}) \sin\theta}}\; e^{j\pi/4} \qquad (c\text{-}3)$$

and

$$\sin\theta = \sin\frac{d}{r_e} = \sin\left(\frac{2\pi r_e - d}{r_e}\right) .$$

If the ionosphere is not isotropic and homogeneous, then a common practice has been to replace the exponential dependence by

$$\alpha' d \rightarrow \int_o^d \alpha_D(r)dr \quad ; \quad \frac{c}{V_{ph}} d \rightarrow \int_o^d \frac{c}{V_{ph}} dr$$

$$\alpha'(2\pi r_e - d) \rightarrow \int_o^{(2\pi r_e - d)} \alpha_R(r)dr \quad ; \quad \text{etc.}$$

resulting in equations 2 and 3 in Section I. It must be mentioned that at present there is no theoretical justification for the simple replacement of exponential terms. However it tends to accentuate the nulls and peaks of the standing wave pattern and hence provides good bounds for the true value of total signal strength $(H_\varphi)_T$. Figure C-1 shows curves of $\left|\frac{(H_\varphi)_D}{F}\right|$ and $\left|\frac{(H_\varphi)_R}{F}\right|$ for various constant values of α_D and α_R. In absence of phase information one can compute the maximum and minimum values of H_T from

$$\frac{|(H_\varphi)_T|_{max}}{|(H_\varphi)_D|} = \frac{|(H_\varphi)_D| + |(H_\varphi)_R}{|(H_\varphi)_D|} \qquad (c-4)$$

$$\frac{|(H_\varphi)_T|_{min}}{|(H_\varphi)_D|} = \frac{|(H_\varphi)_D| - |(H_\varphi)_R|}{|(H_\varphi)_D|} . \qquad c-5)$$

Figure C-2 is a graph of

$$\frac{|(H_\varphi)_T|_{min}}{|(H_\varphi)_D|} \text{ and } \frac{|(H_\varphi)_T|_{max}}{|(H_\varphi)_D|} \text{ versus } \frac{|(H_\varphi)_R|}{|(H_\varphi)_D|}$$

We use these curves in the following ways:

(1) If the attenuation coefficients α_D and α_R are constants one can use curves similar to those in Fig. C-1 to determine $|(H_\varphi)_D|/F$ and $|(H_\varphi)_R|/F$ as well as the ratio $\frac{|(H_\varphi)_R|}{|(H_\varphi)_D|}$. If these are known then the maximum and minimum values of $(H_\varphi)_T$ can be found from Fig. C-2.

(2) If the attenuation coefficients α_D and α_R vary with direction and position then one must use the full equations 2 and 3 of Section I. Then with the use of Fig. C-2 one can compute the maximum and minimum values of $(H_\varphi)_T$.

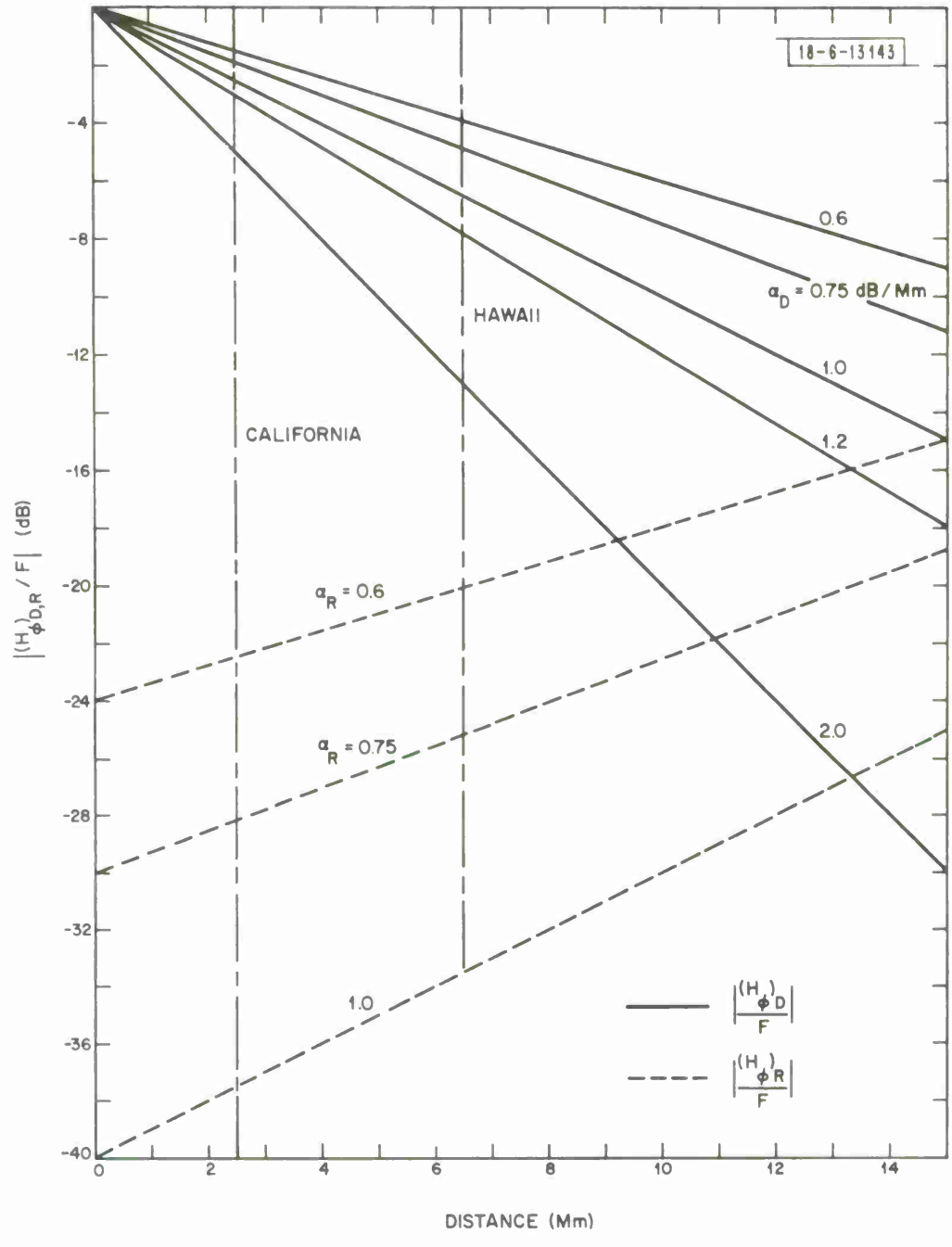

Fig. C-1. Normalized direct and round-the-world field strengths.

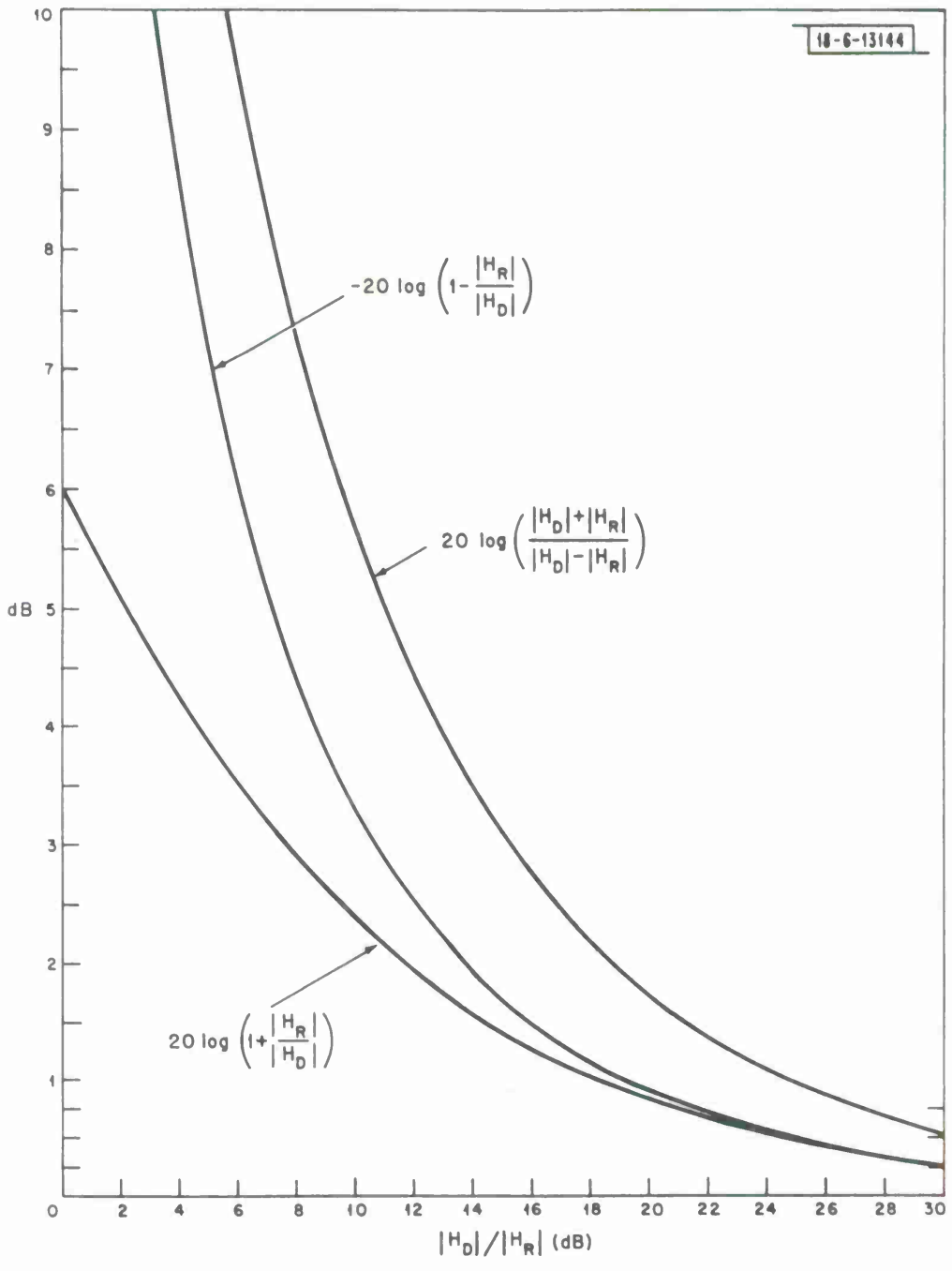

Fig. C-2. Maximum and minimum standing wave interference effects.

APPENDIX D DERIVATION OF A COMPOSITE CONFIDENCE LIMIT FOR $\overline{A^2}$

In the text we have defined the unbiased composite field strength as

$$\overline{A^2} \triangleq \frac{\sum_{i=1}^{M} \frac{(\hat{A_i^2})_u}{N_i}}{\sum_{i=1}^{M} \frac{1}{N_i}} \qquad (\overline{A^2} \triangleq \overline{H_\sigma^2}) \tag{d-1}$$

where N_i is the ith integrated noise estimate and $(\hat{A_i^2})_u$ is the corresponding unbiased estimate for A^2. It is noted that the weighting gives greater weight to those samples which exhibit the higher S/N ratios. The N_i can be determined to a very high degree of accuracy and for purposes of computing a composite confidence limit these values will be considered known constants. The mean and variance of $\overline{A^2}$ then are

$$E[\overline{A^2}] = \frac{\sum_{i=1}^{M} \frac{1}{N_i} E[(\hat{A_i^2})_u]}{\sum_{i=1}^{M} \frac{1}{N_i}} = \frac{\sum_{i=1}^{M} \frac{1}{N_i} A^2}{\sum_{i=1}^{M} \frac{1}{N_i}} = A^2 \tag{d-2}$$

and

$$\text{var}\,(\overline{A^2}) = \frac{\sum_{i=1}^{N} \frac{1}{(N_i)^2} \text{var}\,[(\hat{A_i^2})_u]}{(\sum \frac{1}{N_i})^2} \quad .$$

For the receiver structure exhibited in Fig. 2 it can be shown that

$$\text{var}\,[(\hat{A_i^2})_u] = \text{var}\,[\hat{A_i^2}] = 4\,(N_i^2 + N_i A^2) \tag{d-3}$$

for $A^2/N_i > 10$ we can make the approximation

$$\text{var}\,[(\hat{A_i^2})_u] \simeq 4A^2 N_i \text{ and hence} \tag{d-4}$$

$$\text{var}\,(\overline{A^2}) = \frac{\sum_{i=1}^{N} \frac{4A^2}{N_i}}{\left(\sum_{i=1}^{N} \frac{1}{N_i}\right)^2} = \frac{4A^2}{\left(\sum_{i=1}^{N} \frac{1}{N_i}\right)} = K^2A^2 \qquad \text{(d-5)}$$

where $K^2 = \dfrac{4}{\sum_{i=1}^{M} \frac{1}{N_i}}$.

The random variable $\overline{A^2}$ can be assumed to be Gaussian distributed in the vicinity of the mean A^2

$$f(\overline{A^2};\, A^2) = \frac{1}{\sqrt{2\pi}\, AK}\, e^{-\frac{(\overline{A^2} - A^2)^2}{2(AK)^2}} \qquad \text{(d-6)}$$

The confidence curves are derived from the relationship

$$\int_{(\overline{A^2})_L = -\gamma + A^2}^{(\overline{A^2})_U = \gamma + A^2} f(\overline{A^2};\, A^2)\, d\overline{A^2} = 1 - \epsilon \ . \qquad \text{(d-7)}$$

Let us first provide a normalization by setting $y = \dfrac{\overline{A^2} - A^2}{AK}$. Equation d-7 reduces to

$$\int_{-\frac{\gamma}{AK}}^{\frac{\gamma}{AK}} \left[\frac{1}{\sqrt{2\pi}}\, e^{-\frac{y^2}{2}}\right] dy = 1 - \epsilon \ .$$

The upper and lower bounds are both determined from the following

$$Q\left(\frac{\pm\gamma}{AK}\right) = \pm \int_{\pm\frac{\gamma}{AK}}^{\pm\infty} \left\{\frac{1}{\sqrt{2\pi}}\, e^{-\frac{y^2}{2}}\right\} = \frac{\epsilon}{2} \qquad \text{(d-8)}$$

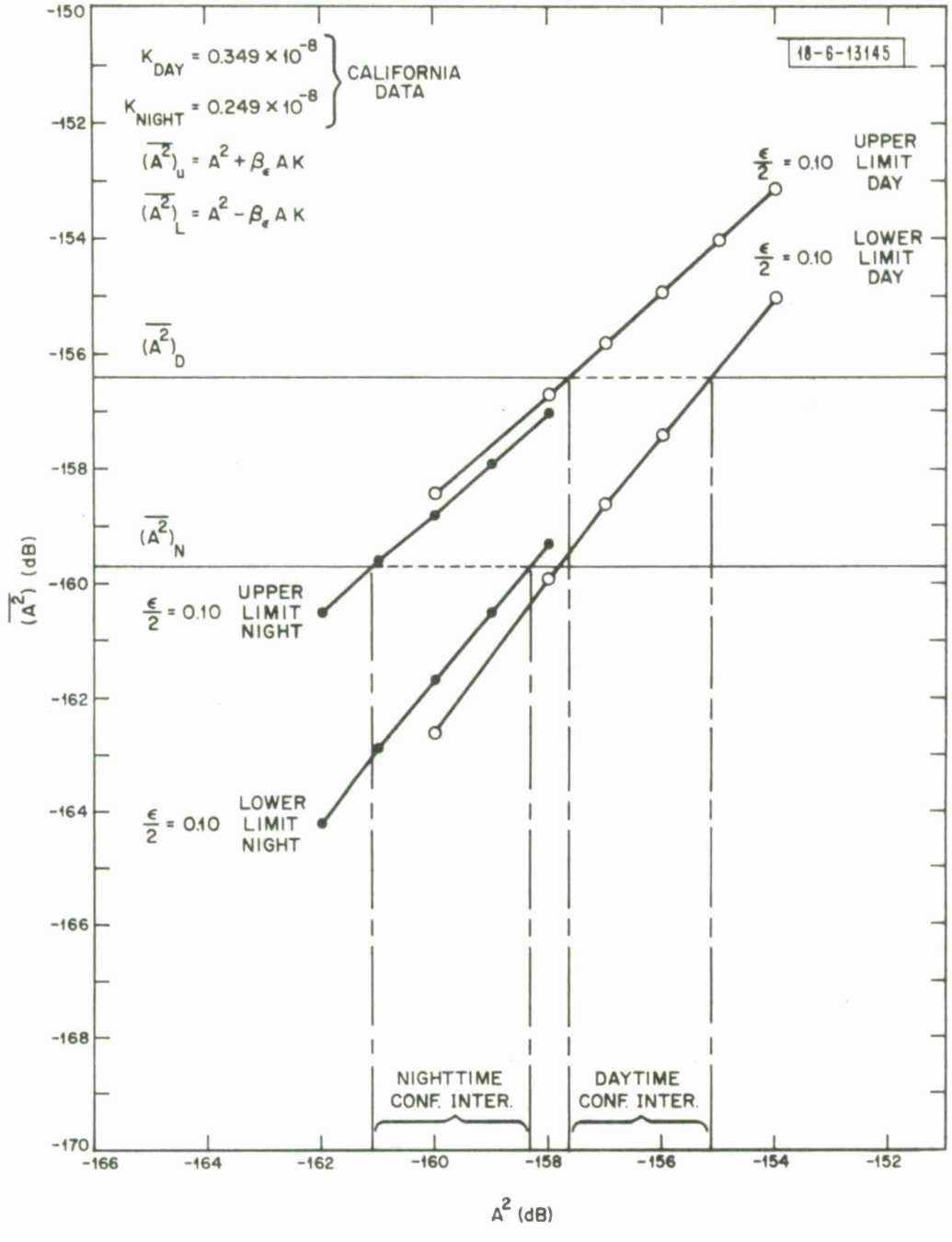

Fig. D-1. Composite confidence curves.

$\frac{\epsilon}{2}$	.10	.05	.025
$\frac{\gamma}{AK} = \beta_\epsilon$	$\beta_\epsilon = 1.28$	$\beta_\epsilon = 1.64$	$\beta_\epsilon = 1.96$

Thus the upper and lower confidence curves are derived from

$$\overline{(A^2)}_U = A^2 + \beta_\epsilon (AK) \qquad \text{(d-9)}$$

$$\overline{(A^2)}_L = A^2 - \beta_\epsilon (AK) \ .$$

Figure D-1 shows typical composite confidence curves for the averaged daytime and nighttime unbiased signal estimate. The confidence intervals (at $\epsilon/2 = .1$) for the composite values $\overline{(A^2)}_D$ and $\overline{(A^2)}_N$ are also shown.

REFERENCES

1. Galejs, J., "F Layer Reflections and Ion Effects in the Propagation of Terrestial ELF Waves," Journal of Geophysical Research, 75, No. 13 (May 1970).

2. Field, E. C., "The Propagation of ELF Waves Under Normal and Naturally Disturbed Conditions," Rand Corporation Document RM-5922-ARPH (March 1969).

3. Smith, E. J., "Propagation of Low-Audio Frequency Waves," Ph. D. Thesis, University of California at Los Angeles, California (February 1960).

4. Hughes, H. and Theisen, J., "Diurnal Variations in the Apparent Attenuations of ELF Atmospherics over Two Different Propagation Paths," Journal of Geophysical Research, 75, No. 15 (May 1970).

5. Wait, J., "Earth-Ionosphere Cavity Resonances and the Propagation of ELF Radio Waves," Radio Science, 69D, No. 8 (August 1965).

6. Holsinger, J., "Confidence Intervals and Sample Sizes in the Measurement of Signal and Noise Powers, Signal-to-Noise Ratios and Probability of Error," M.I.T. Lincoln Laboratory Report 34G-9 (3 January 1963), DDC AD-295133.

7. Van Trees, H. L., "Detection, Estimation and Modulation Theory - 'Part I'," John Wiley and Sons, Inc., New York (1968).

8. Evans, J., Lincoln Laboratory report to be published.

DOCUMENT CONTROL DATA – R&D

(Security classification of title, body of abstract and indexing annotation must be entered when the overall report is classified)

1. ORIGINATING ACTIVITY *(Corporate author)* Lincoln Laboratory, M.I.T.	2a. REPORT SECURITY CLASSIFICATION Unclassified 2b. GROUP None

3. REPORT TITLE

ELF Propagation Study (Phase 1 – Summer 1970)

4. DESCRIPTIVE NOTES *(Type of report and inclusive dates)*

Technical Note

5. AUTHOR(S) *(Last name, first name, initial)*

White, David P. and William, Donald K.

6. REPORT DATE	7a. TOTAL NO. OF PAGES	7b. NO. OF REFS
11 January 1971	56	8

8a. CONTRACT OR GRANT NO. F19628-70-C-0230 b. PROJECT NO. 1508A c. d.	9a. ORIGINATOR'S REPORT NUMBER(S) Technical Note 1971-3 9b. OTHER REPORT NO(S) *(Any other numbers that may be assigned this report)* ESD-TR-71-4

10. AVAILABILITY/LIMITATION NOTICES

This document has been approved for public release and sale; its distribution is unlimited.

11. SUPPLEMENTARY NOTES	12. SPONSORING MILITARY ACTIVITY
None	Department of the Navy

13. ABSTRACT

With the availability of an ELF transmitter (the Bravo test facility at Clam Lake, Wisconsin) it now becomes feasible to make far-field field strength measurements at the lower ELF frequencies. Field strength measurements were made in Hawaii and California at 45 and 75 Hz in an attempt to determine the east-west attenuation rate under daytime or nighttime conditions over the propagation path. As a result of high atmospheric noise conditions and a low transmitted power level, the relatively large uncertainty in signal estimates makes accurate estimation of α impossible. However, the data indicate a daytime east to west attenuation rate between 0.7 and 1.2 db/Mm and a nighttime rate between 1.0 and 1.8 db/Mm.

Future experiments are being planned to refine the estimates of α to within ±0.2 db/Mm.

14. KEY WORDS

ELF propagation | attenuation coefficient | signal-to-noise ratio